



Smoothed particle hydrodynamics calculations of stellar interactions

Frederic A. Rasio^{a,*}, James C. Lombardi Jr.^b

^a*Department of Physics, M.I.T., 77 Massachusetts Av. 6-201, Cambridge, MA 02139, USA*

^b*Department of Physics, Vassar College, Poughkeepsie, NY 12604, USA*

Received 5 May 1998; received in revised form 5 March 1999

Abstract

Smoothed particle hydrodynamics is a multidimensional Lagrangian method of numerical hydrodynamics that has been used to tackle a wide variety of problems in astrophysics. Here we develop the basic equations of the SPH scheme, and we discuss some of its numerical properties and limitations. As an illustration of typical astrophysical applications, we discuss recent calculations of stellar interactions, including collisions between main sequence stars and the coalescence of compact binaries. © 1999 Elsevier Science B.V. All rights reserved.

Keywords: Hydrodynamics; Particle methods; Astrophysics

1. Smoothed particle hydrodynamics

Smoothed particle hydrodynamics (SPH) is a Lagrangian method that was introduced specifically to simulate self-gravitating fluids moving freely in three dimensions. The key idea of SPH is to calculate pressure gradient forces by kernel estimation, directly from the particle positions, rather than by finite differencing on a grid, as in older particle methods such as PIC. SPH was first introduced by Lucy [36] and Gingold and Monaghan [19], who used it to study dynamical fission instabilities in rapidly rotating stars. Since then, a wide variety of astrophysical fluid dynamics problems have been tackled using SPH (see [40] for an overview). In addition to the stellar interaction problems described in Section 2, these have included planet and star formation [45,7] supernova explosions [22,18] large-scale cosmological structure formation [26,59] and galaxy formation [25,64].

* Corresponding author.

E-mail address: rasio@mit.edu (F.A. Rasio)

1.1. SPH from a variational principle

A straightforward derivation of the basic SPH equations can be obtained from a Lagrangian formulation of hydrodynamics [20]. Consider for simplicity the adiabatic evolution of an ideal fluid with equation of state

$$p = A\rho^\gamma, \quad (1)$$

where p is the pressure, ρ is the density, γ is the adiabatic exponent, and A (assumed here to be constant in space and time) is related to the specific entropy ($s \propto \ln A$). The Euler equations of motion

$$\frac{d\mathbf{v}}{dt} = \frac{\partial \mathbf{v}}{\partial t} + (\mathbf{v} \cdot \nabla)\mathbf{v} = -\frac{1}{\rho}\nabla p \quad (2)$$

can be derived from a variational principle with the Lagrangian

$$L = \int \left\{ \frac{1}{2}v^2 - u[\rho(\mathbf{r})] \right\} \rho d^3x. \quad (3)$$

Here $u[\rho] = p/[(\gamma - 1)\rho] = A\rho^{\gamma-1}/(\gamma - 1)$ is the specific internal energy of the fluid.

The basic idea in SPH is to use the discrete representation

$$L_{\text{SPH}} = \sum_{i=1}^N m_i \left[\frac{1}{2}v_i^2 - u(\rho_i) \right] \quad (4)$$

for the Lagrangian, where the sum is over a large but discrete number of small fluid elements, or “particles”, covering the volume of the fluid. Here m_i is the mass and \mathbf{v}_i is the velocity of the particle with position \mathbf{r}_i . For expression (4) to become the Lagrangian of a system with a finite number N of degrees of freedom, we need a prescription to compute the density ρ_i at the position of any given particle i , as a function of the masses and positions of neighboring particles.

In SPH, the density at any position is typically calculated as the local average

$$\rho(\mathbf{r}) = \sum_j m_j W(\mathbf{r} - \mathbf{r}_j; h), \quad (5)$$

where $W(\mathbf{x}; h)$ is an interpolation, or smoothing, kernel of width $\sim h$. Necessary constraints on the kernel $W(\mathbf{x}; h)$ are that (i) it integrates to unity (consequently the integral of Eq. (5) over all space automatically gives the total mass of the system), and (ii) it approaches the Dirac delta function $\delta(\mathbf{x})$ in the limit $h \rightarrow 0$.

Eq. (5) gives, in particular, the density in the vicinity of particle i as $\rho_i = \rho(\mathbf{r}_i)$, and we can now obtain the equations of motion for all the particles. Deriving the Euler–Lagrange equations from L_{SPH} we get

$$\frac{d\mathbf{v}_i}{dt} = - \sum_j m_j \left(\frac{p_i}{\rho_i^2} + \frac{p_j}{\rho_j^2} \right) \nabla_i W_{ij}, \quad (6)$$

where $W_{ij} = W(\mathbf{r}_i - \mathbf{r}_j; h)$ and we have assumed that the form of W is such that $W_{ij} = W_{ji}$. The expression on the right-hand side of Eq. (6) is a sum over neighboring particles (within a distance $\sim h$ of \mathbf{r}_i) representing a discrete approximation to the pressure gradient force $[-(1/\rho)\nabla p]_i$ acting on particle i .

The following energy and momentum conservation laws are satisfied *exactly* by the simple SPH equations of motion given above

$$\frac{d}{dt} \left(\sum_{i=1}^N m_i \mathbf{v}_i \right) = 0 \quad (7)$$

and

$$\frac{d}{dt} \left(\sum_{i=1}^N m_i \left[\frac{1}{2} v_i^2 + u_i \right] \right) = 0, \quad (8)$$

where $u_i = p_i/[(\gamma - 1)\rho_i]$. Note that energy and momentum conservation in this simple version of SPH is independent of the number of particles N .

Typically, a full implementation of SPH for astrophysical problems will add to Eq. (6) a treatment of self-gravity (e.g., using one of the many grid-based or tree-based algorithms developed for N -body simulations) and an artificial viscosity term to allow for entropy production in shocks. In addition, we have assumed here that the smoothing length h is constant in time and the same for all particles. In practice, individual and time-varying smoothing lengths $h_i(t)$ are almost always used, so that the local spatial resolution can be adapted to the (time-varying) density of SPH particles (see [46] for a rigorous derivation of the equations of motion from a variational principle in this case). Other derivations of the SPH equations, based on the application of smoothing operators to the fluid equations (and without the use of a variational principle), are also possible (see, e.g., [24]).

1.2. Basic SPH equations

In this section, we summarize the basic equations for various forms of the SPH scheme currently in use, incorporating gravity, artificial viscosity, and individual smoothing lengths.

1.2.1. Density and pressure

The SPH estimate of the fluid density at \mathbf{r}_i is calculated as $\rho_i = \sum_j m_j W_{ij}$ [cf. Eq. (5)]. Many recent implementations of SPH use a form for W_{ij} proposed by Hernquist and Katz [24]:

$$W_{ij} = \frac{1}{2} [W(|\mathbf{r}_i - \mathbf{r}_j|; h_i) + W(|\mathbf{r}_i - \mathbf{r}_j|; h_j)]. \quad (9)$$

This choice guarantees symmetric weights $W_{ij} = W_{ji}$ even between particles i and j with different smoothing lengths. For the interpolation kernel $W(r; h)$, the cubic spline

$$W(r; h) = \frac{1}{\pi h^3} \begin{cases} 1 - \frac{3}{2} \left(\frac{r}{h}\right)^2 + \frac{3}{4} \left(\frac{r}{h}\right)^3, & 0 \leq \frac{r}{h} < 1, \\ \frac{1}{4} [2 - \left(\frac{r}{h}\right)]^3, & 1 \leq \frac{r}{h} < 2, \\ 0, & \frac{r}{h} \geq 2, \end{cases} \quad (10)$$

[41] is a common choice. Eq. (10) is sometimes called a “second-order accurate” kernel. Indeed, when the true density $\rho(\mathbf{r})$ of the fluid is represented by an appropriate distribution of particle positions, masses, and smoothing lengths, one can show that $\rho_i = \rho(\mathbf{r}_i) + O(h_i^2)$ (see, e.g., [38]).

Depending on which thermodynamic evolution equation is integrated [see Eqs. (26) and (27) below], particle i also carries either the parameter u_i , the internal energy per unit mass in the fluid at \mathbf{r}_i , or A_i , the entropic variable, a function of the specific entropy in the fluid at \mathbf{r}_i . Although

arbitrary equations of state can be implemented in SPH, here, for simplicity, we consider only polytropic equations of state. The pressure p_i at \mathbf{r}_i is therefore related to the density by

$$p_i = (\gamma - 1)\rho_i u_i \quad (11)$$

or

$$p_i = A_i \rho_i^\gamma. \quad (12)$$

The speed of sound in the fluid at \mathbf{r}_i is $c_i = (\gamma p_i / \rho_i)^{1/2}$.

1.2.2. Dynamical equations and gravity

Particle positions are updated either by

$$\frac{d\mathbf{r}_i}{dt} = \mathbf{v}_i \quad (13)$$

or the more general XSPH method

$$\frac{d\mathbf{r}_i}{dt} = \mathbf{v}_i + \varepsilon \sum_j m_j \frac{\mathbf{v}_j - \mathbf{v}_i}{\rho_{ij}} W_{ij}, \quad (14)$$

where $\rho_{ij} = (\rho_i + \rho_j)/2$ and ε is a constant parameter in the range $0 < \varepsilon < 1$ [39]. Eq. (14), in contrast to Eq. (13), changes particle positions at a rate closer to the local smoothed velocity. The XSPH method was originally proposed as a way to minimize spurious interparticle penetration across the interface of two colliding fluid streams.

Generalizing Eq. (6) to account for gravitational forces and artificial viscosity (hereafter AV), the velocity of particle i is updated according to

$$\frac{d\mathbf{v}_i}{dt} = \mathbf{a}_i^{(\text{Grav})} + \mathbf{a}_i^{(\text{SPH})}, \quad (15)$$

where $\mathbf{a}_i^{(\text{Grav})}$ is the gravitational acceleration and

$$\mathbf{a}_i^{(\text{SPH})} = - \sum_j m_j \left[\left(\frac{p_i}{\rho_i^2} + \frac{p_j}{\rho_j^2} \right) + \Pi_{ij} \right] \nabla_i W_{ij}. \quad (16)$$

Various forms for the AV term Π_{ij} are discussed below. The AV ensures that correct jump conditions are satisfied across (smoothed) shock fronts, while the rest of Eq. (16) represents one of many possible SPH-estimators for the acceleration due to the local pressure gradient (see, e.g., [38]).

To provide reasonable accuracy, an SPH code must solve the equations of motion of a large number of particles (typically $N \gg 1000$). This rules out a direct summation method for calculating the gravitational field of the system, unless special purpose hardware such as the GRAPE is used [64,27]. In most implementations of SPH, particle-mesh algorithms [16,53,10] or tree-based algorithms [24,13] are used to calculate the gravitational accelerations $\mathbf{a}_i^{(\text{Grav})}$. Tree-based algorithms perform better for problems involving large dynamic ranges in density, such as star formation and large-scale cosmological simulations. For stellar interaction problems like those described in Section 2, density contrasts rarely exceed a factor $\sim 10^2$ – 10^3 and in those cases grid-based algorithms and direct solvers are generally faster. Tree-based and grid-based algorithms are also used to calculate lists of nearest neighbors for each particle exactly as in gravitational N -body simulations.

1.2.3. Artificial viscosity

For the AV, a symmetrized version of the form proposed by Monaghan [39] is often adopted:

$$\Pi_{ij} = \frac{-\alpha\mu_{ij}c_{ij} + \beta\mu_{ij}^2}{\rho_{ij}}, \quad (17)$$

where α and β are constant parameters, $c_{ij} = (c_i + c_j)/2$, and

$$\mu_{ij} = \begin{cases} \frac{(\mathbf{v}_i - \mathbf{v}_j) \cdot (\mathbf{r}_i - \mathbf{r}_j)}{h_{ij}(|\mathbf{r}_i - \mathbf{r}_j|^2/h_{ij}^2 + \eta^2)} & \text{if } (\mathbf{v}_i - \mathbf{v}_j) \cdot (\mathbf{r}_i - \mathbf{r}_j) < 0, \\ 0 & \text{if } (\mathbf{v}_i - \mathbf{v}_j) \cdot (\mathbf{r}_i - \mathbf{r}_j) \geq 0 \end{cases} \quad (18)$$

with $h_{ij} = (h_i + h_j)/2$. This form represents a combination of a bulk viscosity (linear in μ_{ij}) and a von Neumann–Richtmyer viscosity (quadratic in μ_{ij}). The von Neumann–Richtmyer viscosity was initially introduced to suppress particle interpenetration in the presence of strong shocks. Eq. (17) provides a good treatment of shocks when $\alpha \approx 1$, $\beta \approx 2$ and $\eta^2 \sim 10^{-2}$ [39,24].

A well-known problem with the classical AV of Eq. (17) is that it can generate large amounts of spurious shear viscosity. For this reason, Hernquist and Katz [24] introduced another form for the AV:

$$\Pi_{ij} = \begin{cases} \frac{q_i}{\rho_i^2} + \frac{q_j}{\rho_j^2} & \text{if } (\mathbf{v}_i - \mathbf{v}_j) \cdot (\mathbf{r}_i - \mathbf{r}_j) < 0, \\ 0 & \text{if } (\mathbf{v}_i - \mathbf{v}_j) \cdot (\mathbf{r}_i - \mathbf{r}_j) \geq 0, \end{cases} \quad (19)$$

where

$$q_i = \begin{cases} \alpha\rho_i c_i h_i |\nabla \cdot \mathbf{v}|_i + \beta\rho_i h_i^2 |\nabla \cdot \mathbf{v}|_i^2 & \text{if } (\nabla \cdot \mathbf{v})_i < 0, \\ 0 & \text{if } (\nabla \cdot \mathbf{v})_i \geq 0 \end{cases} \quad (20)$$

and

$$(\nabla \cdot \mathbf{v})_i = \frac{1}{\rho_i} \sum_j m_j (\mathbf{v}_j - \mathbf{v}_i) \cdot \nabla_i W_{ij}. \quad (21)$$

Although this form provides a slightly less accurate description of shocks than Eq. (17), it does exhibit less shear viscosity.

More recently, Balsara [2] has proposed the AV

$$\Pi_{ij} = \left(\frac{p_i}{\rho_i^2} + \frac{p_j}{\rho_j^2} \right) (-\alpha\mu_{ij} + \beta\mu_{ij}^2), \quad (22)$$

where

$$\mu_{ij} = \begin{cases} \frac{(\mathbf{v}_i - \mathbf{v}_j) \cdot (\mathbf{r}_i - \mathbf{r}_j)}{h_{ij}(|\mathbf{r}_i - \mathbf{r}_j|^2/h_{ij}^2 + \eta^2)} \frac{f_i + f_j}{2c_{ij}} & \text{if } (\mathbf{v}_i - \mathbf{v}_j) \cdot (\mathbf{r}_i - \mathbf{r}_j) < 0, \\ 0 & \text{if } (\mathbf{v}_i - \mathbf{v}_j) \cdot (\mathbf{r}_i - \mathbf{r}_j) \geq 0. \end{cases} \quad (23)$$

Here f_i is the form function for particle i defined by

$$f_i = \frac{|\nabla \cdot \mathbf{v}|_i}{|\nabla \cdot \mathbf{v}|_i + |\nabla \times \mathbf{v}|_i + \eta' c_i / h_i}, \quad (24)$$

where the factor $\eta' \sim 10^{-4} - 10^{-5}$ prevents numerical divergences, $(\nabla \cdot \mathbf{v})_i$ is given by Eq. (21), and

$$(\nabla \times \mathbf{v})_i = \frac{1}{\rho_i} \sum_j m_j (\mathbf{v}_i - \mathbf{v}_j) \times \nabla_i W_{ij}. \quad (25)$$

The form function f_i acts as a switch, approaching unity in regions of strong compression ($|\nabla \cdot \mathbf{v}|_i \gg |\nabla \times \mathbf{v}|_i$) and vanishing in regions of large vorticity ($|\nabla \times \mathbf{v}|_i \gg |\nabla \cdot \mathbf{v}|_i$). Consequently, this AV has the advantage that it is suppressed in shear layers. Note that since $(p_i/\rho_i^2 + p_j/\rho_j^2) \approx 2c_{ij}^2/(\gamma\rho_{ij})$, Eq. (22) behaves like Eq. (17) when $|\nabla \cdot \mathbf{v}|_i \gg |\nabla \times \mathbf{v}|_i$, provided one rescales the α and β in Eq. (22) to be a factor of $\gamma/2$ times the α and β in Eq. (17).

1.2.4. Thermodynamics

To complete the description of the fluid, either u_i or A_i is evolved according to a discretized version of the first law of thermodynamics. Although various forms of these evolution equations exist, the most commonly used are

$$\frac{du_i}{dt} = \frac{1}{2} \sum_j m_j \left(\frac{p_i}{\rho_i^2} + \frac{p_j}{\rho_j^2} + \Pi_{ij} \right) (\mathbf{v}_i - \mathbf{v}_j) \cdot \nabla_i W_{ij} \quad (26)$$

and

$$\frac{dA_i}{dt} = \frac{\gamma - 1}{2\rho_i^{\gamma-1}} \sum_j m_j \Pi_{ij} (\mathbf{v}_i - \mathbf{v}_j) \cdot \nabla_i W_{ij}. \quad (27)$$

We call Eq. (26) the “energy equation”, while Eq. (27) is the “entropy equation”. Which equation one should integrate depends upon the problem being treated. Each has its own advantages and disadvantages. Note that the derivation of Eqs. (26) and (27) neglects terms proportional to the time derivative of h_i . Therefore if we integrate the energy equation, even in the absence of AV, the total entropy of the system will not be strictly conserved if the particle smoothing lengths are allowed to vary in time; if the entropy equation is used to evolve the system, the total entropy would then be strictly conserved when $\Pi_{ij} = 0$, but not the total energy [49,23]. For more accurate treatments involving time-dependent smoothing lengths, see [46,58]. The energy equation has the advantage that other thermodynamic processes such as heating and cooling [26] and nuclear burning [18] can be incorporated more easily.

1.2.5. Integration in time

The results of SPH simulations involving only hydrodynamic forces and gravity do not depend strongly on the actual time-stepping routine used, as long as the routine remains stable and accurate. A simple second-order explicit leap-frog scheme is often employed. Implicit schemes must be used when other processes such as heating and cooling are coupled to the dynamics [26]. A low-order scheme is appropriate for SPH because pressure gradient forces are subject to numerical noise. For stability, the timestep must satisfy a modified Courant condition, with h_i replacing the usual grid separation. For accuracy, the timestep must be a small enough fraction of the dynamical time.

Among the many possible choices for determining the timestep, the prescription proposed by Monaghan [39] is recommended. This sets

$$\Delta t = C_N \text{Min}(\Delta t_1, \Delta t_2), \quad (28)$$

where the constant dimensionless Courant number C_N typically satisfies $0.1 \lesssim C_N \lesssim 0.8$, and where

$$\Delta t_1 = \text{Min}_i (h_i / \dot{v}_i)^{1/2}, \quad (29)$$

$$\Delta t_2 = \text{Min}_i \left(\frac{h_i}{c_i + k(\alpha c_i + \beta \text{Max}_j |\mu_{ij}|)} \right) \quad (30)$$

with k being a constant of order unity. If the Hernquist and Katz AV [Eq. (19)] is used, the quantity $\text{Max}_j |\mu_{ij}|$ in Eq. (30) can be replaced by $h_i |\nabla \cdot \mathbf{v}|_i$ if $(\nabla \cdot \mathbf{v})_i < 0$, and by 0 otherwise. By accounting for AV-induced diffusion, the α and β terms in the denominator of Eq. (30) allow for a more efficient use of computational resources than simply using a smaller value of C_N .

1.2.6. Smoothing lengths and accuracy

The size of the smoothing lengths is often chosen such that particles roughly maintain some predetermined number of neighbors N_N . Typical values of N_N range from about 20–100. If a particle interacts with too few neighbors, then the forces on it are sporadic, a poor approximation to the forces on a true fluid element. In general, one finds that, for given physical conditions, the noise level in a calculation always decreases when N_N is increased.

At the other extreme, large neighbor numbers degrade the resolution by requiring unreasonably large smoothing lengths. However, higher accuracy is obtained in SPH calculations only when *both* the number of particles N and the number of neighbors N_N are increased, with N increasing faster than N_N so that the smoothing lengths h_i decrease. Otherwise (e.g., if N is increased while maintaining N_N constant) the SPH method is *inconsistent*, i.e., it converges to an unphysical limit. This can be shown easily by deriving the dispersion relation for sound waves propagating in simple SPH systems [49]. The choice of N_N for a given calculation is therefore dictated by a compromise between an acceptable level of numerical noise and the desired spatial resolution (which is $\approx h \propto 1/N_N^{1/d}$ in d dimensions) and level of accuracy.

1.3. Results of recent test calculations

The authors and their collaborators have performed a series of systematic tests to evaluate the effects of spurious transport in SPH calculations. These tests are presented in detail in [35], while here we summarize the main results. Our tests include (i) particle diffusion measurements, (ii) shock-tube tests, (iii) numerical viscosity measurements, and (iv) measurements of the spurious transport of angular momentum due to AV in differentially rotating, self-gravitating configurations. The results are useful for quantifying the accuracy of the SPH scheme, especially for problems where shear flows or shocks are present, as well as for problems where true mixing is relevant. Other recent tests of SPH include those by Hernquist and Katz [24] and by Steinmetz and Müller [65].

1.3.1. Particle diffusion

Many of our tests focus on spurious diffusion, the motion of SPH particles introduced as an artifact of the numerical scheme. Often applications require a careful tracing of the particle positions, and in these cases it is essential that spurious diffusion be small. For example, SPH simulations can be used to establish the degree of fluid mixing during stellar collisions, which is of primary importance

in determining the subsequent stellar evolution of the merger remnants (see Section 2.1). It must be stressed that the amount of mixing determined by SPH calculations is always an upper limit. In particular, low-resolution calculations tend to be noisy, and this noise can lead to spurious diffusion of particles, independent of any real physical mixing of fluid elements.

We have analyzed spurious diffusion by using SPH particles in a box with periodic boundary conditions to model a stationary fluid of infinite extent. For various noise levels (particle velocity dispersions) and neighbor numbers N_N , we measure the rate of diffusion, quantified by the diffusion coefficient

$$D \equiv \left\langle \frac{d\Delta r^2}{dt} \right\rangle. \quad (31)$$

Here the brackets $\langle \rangle$ denote a time average, and $\Delta r = (\Delta x^2 + \Delta y^2 + \Delta z^2)^{1/2}$ is the total distance traveled by a particle due to spurious diffusion. Although strong shocks and AV in SPH calculations can lead to additional particle mixing [39], particle diffusion is the dominant contribution to spurious mixing in weakly shocked fluids.

Once expressed in terms of the number density of SPH particles and the sound speed, these diffusion coefficients can therefore be used to estimate spurious deviations in particle positions in a wide variety of applications, including self-gravitating systems. For each particle in some large-scale simulation, this spurious deviation is estimated simply by numerically integrating

$$\Delta r^2 \approx \int D dt. \quad (32)$$

The coefficient D in the integrand of Eq. (32) depends on the particle's velocity deviation from the local flow, the local number density n of particles, and the local sound speed c_s , so that these quantities need to be monitored for each particle during the simulation. Such a scheme was successfully used to estimate spurious mixing in the context of stellar collisions [33], where typically (with $N = 3 \times 10^4$ and $N_N \approx 64$) the diffusion coefficient was very roughly $D \sim 0.05 c_s n^{-1/3}$.

For sufficiently low noise levels, the diffusion coefficient essentially vanishes, as the particles simply oscillate around equilibrium lattice sites. We say that such a system has “crystallized”. For a neighbor number $N_N \approx 64$, a system of SPH particles will crystallize if the root-mean-square velocity dispersion is less than about 3–4% of the sound speed. We find that crystallized cubic lattices are unstable against perturbations, while lattice types with large packing fractions, such as hexagonal close-packed, are stable. For this reason it may sometimes be better to construct initial data by placing particles in an hexagonal close-packed lattice, rather than in a cubic lattice as is often done.

The diffusion coefficients have been measured using equal-mass particles. Sometimes, however, SPH simulations use particles of unequal mass so that less-dense regions can still be highly resolved. To test the effects of unequal mass particles in a self-gravitating system, we constructed an equilibrium $n = 1.5$ polytrope (a polytrope is an idealized model for a spherical star, characterized by a relation of the form $P = \rho^\gamma$ between pressure P and density ρ ; the polytropic index n is defined by $\gamma = 1 + 1/n$), using particle masses which increased with radius in the initial configuration. Allowing the system to evolve, we observed that the heaviest particles gradually migrated towards the center of the star, exchanging places with less massive particles. For a polytrope modeled with $N \approx 1.4 \times 10^4$ particles and a neighbor number $N_N \approx 64$, the distribution of particle masses is reversed

within roughly 80 dynamical timescales. This is caused by the interactions among neighboring particles via the smoothing kernel. These interactions allow energy exchange, and equipartition of energy then requires the heavier particles to sink into the gravitational potential well. Spurious mixing is therefore a more complicated process in simulations which use unequal mass particles: each particle has a preferred direction to migrate, and in a dynamical application this direction can be continually changing. For simulations in which fluid mixing is important, equal-mass particles are an appropriate choice.

1.3.2. Shock tube tests

The diffusion tests just described are all done in the absence of shocks and without AV. To test the AV schemes described in Section 1.2, we turn to a periodic version of the 1-D Riemann shock-tube problem. Initially, fluid slabs with constant (and alternating) density ρ and pressure p are separated by an infinite number of planar, parallel, and equally spaced interfaces. We treat this inherently 1-D problem with both a 1-D and a 3-D SPH code. The 1-D code is naturally more accurate, and provides a benchmark against which we can compare the results of our 3-D code. In both cases, periodic boundary conditions allow us to model the infinite number of slabs.

Using various values of α and β , we performed a number of such shock tube calculations with our 3-D code, at both Mach numbers $\mathcal{M} \approx 1.6$ and 13.2. We then compared the time variation of the internal energy and entropy of the system against that of the 1-D simulation. Furthermore, since any motion perpendicular to the bulk fluid flow is spurious, we were also able to examine spurious mixing in these simulations. We find that all three forms of AV can handle shocks well. For example, with $N = 10^4$ and $N_N \approx 64$, there is better than 2% agreement with the 1-D code's internal energy vs. time curve when $\mathcal{M} \approx 1.6$, and agreement at about the 3% level when $\mathcal{M} \approx 13.2$. We also find that both Eqs. (17) and (22), as compared to Eq. (19), allow less-spurious mixing and do somewhat better at reproducing the 1-D code's results.

Such simulations are a useful and realistic way to calibrate spurious transport, since the test problem, which includes shocks and significant fluid motion, has many of the same properties as real astrophysical problems. In fact, the recoil shocks in stellar collisions do tend to be nearly planar, so that even the 1-D geometry of the shock fronts is realistic. The periodic boundary conditions play the role of gravity in the sense that they prevent the gas from expanding to infinity.

1.3.3. Shear flows

To test the various AV forms in the presence of a shear flow, we impose the so-called slipping boundary conditions on a periodic box, as is commonly done in molecular dynamics (see, e.g., [42]). The resulting “stationary Couette flow” has a velocity field close to $(v_x, v_y, v_z) = (v_0 y/L, 0, 0)$ and allows us to measure the numerical viscosity of the particles. As in the shock tube tests, we also examine spurious mixing in the direction perpendicular to the fluid flow. These shear tests therefore allow us to further investigate the accuracy of our SPH code as a function of the AV parameters and scheme. We find that both the Hernquist & Katz AV [Eq. (19)] and the Balsara AV [Eq. (22)] exhibit less viscosity than the classical AV [Eq. (17)]. However, the classical AV does allow significantly less spurious mixing than the other forms. For all three forms of the AV,

increasing α and β tends to damp out the noise and consequently decrease spurious mixing, but it also increases the spurious shear viscosity.

Rotation plays an important role in many hydrodynamic processes. For instance, a collision between stars can yield a rapidly and differentially rotating merger remnant. Even in the absence of shocks, AV tends to damp away differential rotation due to the relative velocity of neighboring particles at slightly different radii, and an initially differentially rotating system will tend towards rigid rotation on the viscous dissipation timescale. In systems best modeled with a perfect fluid, ideally with a viscous timescale $\tau = \infty$, any such angular momentum transport introduced by the SPH scheme is spurious.

As a concrete example, we consider an axisymmetric equilibrium configuration differentially rotating with an angular velocity profile $\Omega(\varpi) \propto \varpi^{-\lambda}$, where ϖ is the distance from the rotation axis and λ is a constant of order unity. We then analytically estimate the viscous dissipation timescale for each of the three AVs discussed in Section 1.2. These analytic estimates are found to closely match numerically measured values of the timescale. Both the Hernquist and Katz AV [Eq. (19)] and the Balsara AV [Eq. (22)] yield longer viscous timescales than the classical AV [Eq. (17)], and hence are better at maintaining the angular velocity profile. The Balsara AV clearly does best in this regard, with a viscous timescale roughly $N_N^{1/2}$ times larger than for the classical AV.

When choosing values of AV parameters, one must weigh the relative importance of shocks, shear, and fluid mixing. For this reason, it is an application-dependent, somewhat subjective matter to specify “optimal values” of α and β . We do, however, roughly delineate the boundaries of the region in parameter space that gives acceptable results in [35].

Our results concerning the various AV forms can be summarized as follows (see [35] for more details). We find that the AVs defined by Eqs. (17) and (22) do equally well both in their handling of shocks and in their controlling of spurious mixing, and do slightly better than Eq. (19). Furthermore, both Eqs. (19) and (22) do introduce less numerical viscosity than Eq. (17). Since Eq. (22), Balsara’s form of AV, does indeed significantly decrease the amount of shear viscosity without sacrificing accuracy in the treatment of shocks, we conclude that it is an appropriate choice for a broad range of problems. This is consistent with the successful use of Balsara’s AV reported by Navarro and Steinmetz [44] in their models of rotating galaxies.

2. SPH calculations of stellar interactions

The vast majority of recent 3-D calculations of dynamical interactions between stars have been done using the SPH method. These include collisions [5,33], binary coalescence [14,55], common envelope evolution [52,68], accretion flows [3,69], and tidal disruption [28].

SPH has many advantages over more traditional methods of numerical hydrodynamics for these calculations. First, and perhaps most importantly, the *advection* of the fluid while the stars are moving along their initial trajectories is handled very easily by SPH. For example, in the case of binary coalescence (see Section 2.2 below), one often has to follow the motion of the two stars for several orbital periods before the final merger occurs. Merely tracking the motion of a star across a large 3-D grid for many dynamical times can be very challenging when using an Eulerian scheme, especially in the presence of a sharp stellar surface (as in the case of neutron stars,

which contain a fairly incompressible fluid). In addition, other physical processes can be studied much more easily using a Lagrangian scheme. An example is *hydrodynamic mixing*, which is a crucial process in the study of certain stellar merger processes (see Section 2.1). Since chemical abundances are passively advected quantities during a dynamical evolution, the chemical composition in the final fluid configuration can be determined after the completion of a calculation simply by noting the original and final positions of all SPH particles and by assigning particle abundances according to an initial profile. The adaptiveness of the scheme, with particles automatically concentrating in regions of higher density is also an important advantage, although this is more crucial in situations involving large density contrasts, such as in simulations of star formation or galaxy formation.

2.1. Stellar collisions

As a first illustration of the use of SPH for a typical stellar interaction problem, we summarize in this section recent work on the numerical calculation of collisions between two main-sequence stars.

2.1.1. Motivation

Close dissipative encounters and direct physical collisions between stars occur frequently in dense star clusters. The dissipation of kinetic energy in close stellar encounters can have a direct influence on the overall dynamical evolution of a cluster. Observational evidence for stellar collisions and mergers in globular clusters is provided by the existence of large numbers of *blue stragglers* in these systems. These are peculiar main-sequence (hydrogen burning) stars that appear younger and more massive than all other, normal main-sequence stars in the cluster.

Blue stragglers have long been thought to be formed through the merger of two lower-mass stars, either in a collision or following binary coalescence (see, e.g., the review by Livio [31]). Clear indication for a collisional origin of blue stragglers has come from observations of globular clusters with the Hubble Space Telescope. Large numbers of blue stragglers were found to be concentrated in the cores of the densest clusters (such as M15 and M30).

Following early numerical work in 2-D (e.g., [61]), Benz and Hills [4,5] performed the first 3-D calculations of direct collisions between two main sequence stars using SPH. An important result of this pioneering study was that collisions could lead to a thoroughly mixed merger remnant. The mixing of fresh hydrogen fuel into the core of the remnant could then reset its nuclear clock, allowing the blue straggler to burn hydrogen for a full main-sequence lifetime ($t_{\text{MS}} \sim 10^9$ yr) after its formation.

2.1.2. Recent results using SPH

The authors and their collaborators have re-examined collisions between main-sequence stars, and, in particular, the question of mixing during mergers, by performing a set of numerical hydrodynamic calculations using SPH [32,33,63,62]. This new work differs from the previous study of Benz and Hills [4] by adopting more realistic models of globular cluster stars, and by performing numerical calculations with increased spatial resolution.

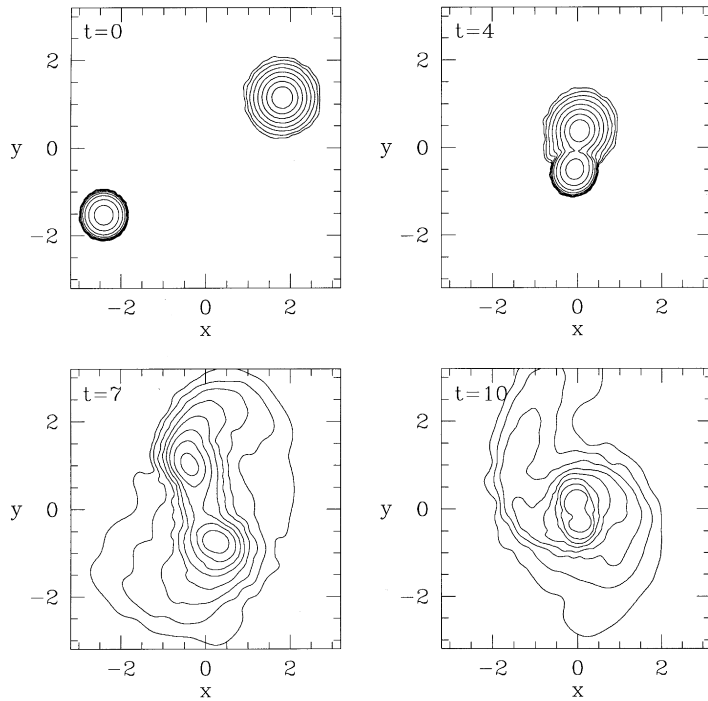


Fig. 1. Snapshots of density contours in the orbital plane for a parabolic collision between two main-sequence stars of masses M_1 and $M_2 = 0.75M_1$. The impact parameter has been chosen such that the corresponding point-mass orbit would have a pericenter separation $r_p = 0.25(R_1 + R_2)$, where R_1 and $R_2 = 0.56R_1$ are the stellar radii. There are eight density contours, which are spaced logarithmically and cover four decades down from the maximum. The elapsed time in the upper left corner of each frame is in units of the dynamical timescale $(R_1^3/GM_1)^{1/2}$. Adapted from Lombardi et al. [33].

Snapshots from one of our recent calculations are shown in Fig. 1. The main new results of these SPH calculations can be summarized as follows. Merger remnants produced by parabolic collisions are always far from chemically homogeneous. In the case of collisions between two nearly identical stars, the amount of hydrodynamic mixing during the collision is minimal. In fact, the final chemical composition profile is very close to the initial profile of the parent stars. For two turnoff stars (i.e., close to hydrogen exhaustion at the center), this means that the merger remnant is born with very little hydrogen to burn in its core and, consequently, that the object may not be able to remain on the main sequence for long. In the case of a collision between two stars of different masses, the chemical composition profile of the merger remnant tends to be more homogeneous, but it remains true that little hydrogen is injected into its core.

At a qualitative level, these results can be understood very simply in terms of the requirement of convective (dynamical) stability of the final hydrostatic equilibrium configurations. For non-rotating remnants, convective stability requires that the entropic variable \mathcal{A} [see Eq. (1)] increase monotonically from the center to the surface (the so-called Ledoux criterion). If shock-heating could be neglected entirely (which is not unreasonable for the low-velocity collisions occurring in globular

clusters), then one could predict the final composition profile of a merger remnant simply by observing the composition and A profiles of the parent stars. Since fluid elements conserve both their value of A (in the absence of shocks) and their composition, the final composition profile of a remnant is constructed simply by combining mass shells in order of increasing A , from the center to the outside. Many features of the results follow directly. For example, in the case of a collision between two identical stars, it is obvious why the composition profile of the merger remnant remains very similar to that of the parent stars, since shock-heating is significant only in the outer layers of the stars, which contain a very small fraction of the total mass. Furthermore, the dense, helium-rich material is concentrated in the deep interior of the parent stars, where shock-heating is negligible, and therefore it remains concentrated in the deep interior of the final configuration.

2.2. Coalescing compact binaries

As a second illustration of the use of SPH for calculations of stellar interactions, we now turn to the dynamical evolution of compact binary star systems (containing two compact objects — black holes or neutron stars — in orbit around one another).

2.2.1. Motivation

Coalescing compact binaries are the most promising known sources of *gravitational radiation* that could be detected by the new generation of laser interferometers now under construction. These include the Caltech-MIT LIGO [1,11] and the European projects VIRGO [6] and GEO 600 [12]. In addition to providing a major new confirmation of Einstein's theory of general relativity, including the first direct proof of the existence of black holes [17], the detection of gravitational waves from coalescing binaries at cosmological distances could provide accurate independent measurements of the Hubble constant and mean density of the universe [57,9,37]. For an excellent recent review on the detection and sources of gravitational radiation, see Thorne [70]. Coalescing compact binaries are important for other areas of astrophysics as well. In particular, many theoretical models of *gamma-ray bursts* have postulated that the energy source for the bursts could be coalescing compact binaries at cosmological distances [15,43]. For a discussion of the hydrodynamics of binary coalescence in the context of gamma-ray burst models, see [56] and references therein.

Here we focus on binaries containing two neutron stars (hereafter NS), for which the final coalescence is a purely hydrodynamic process that has been well-studied using SPH (as well as other methods).

2.2.2. Hydrodynamics of the binary merger process

Hydrostatic equilibrium configurations for binary systems with sufficiently close components can become *dynamically unstable* [8,66]. The physical nature of this instability is common to all binary interaction potentials that are sufficiently steeper than $1/r$ (see, e.g., [21, Section 3.6]). It is analogous to the familiar instability of test particles in circular orbits sufficiently close to a black hole [60, Section 12.4]. Here, however, it is the *tidal interaction* that is responsible for the steepening of the effective interaction potential between the two stars and for the destabilization

of the circular orbit. The physical properties of this instability, and its consequences for NS binary coalescence, have been studied by the authors and their collaborators, both numerically using SPH ([54,55], hereafter RS; [51]), and using analytical perturbation methods ([29,30], hereafter LRS, [34]).

The instability was first identified by RS using SPH calculations where the evolution of binary equilibrium configurations was calculated for two identical polytropes with $\gamma = 2$. It was found that when $r \lesssim 3R$ (r is the binary separation and R the radius of an unperturbed NS), the orbit becomes unstable to radial perturbations and the two stars undergo rapid coalescence. For $r \gtrsim 3R$, the system could be evolved dynamically for many orbital periods without showing any sign of orbital evolution (in the absence of dissipation). Many of the results derived in RS and LRS concerning the stability properties of NS binaries have been confirmed recently in completely independent work by New and Tohline [47] and by Zhuge et al. [72]. New and Tohline [47] used completely different numerical methods (a combination of a 3-D Self-Consistent Field code for constructing equilibrium configurations and a grid-based Eulerian code for following the dynamical evolution of the binaries), while Zhuge et al. [72] used SPH.

2.2.3. Typical SPH results

For simplicity, we describe here the dynamical evolution of an unstable, initially synchronized binary containing two identical stars. Typical SPH results for this case are shown in Fig. 2. During the initial, linear stage of the instability, the two stars approach each other and come into contact after about one orbital revolution. In the corotating frame of the binary, the relative velocity remains very subsonic, so that the evolution is adiabatic at this stage. This is in sharp contrast to the case of a head-on collision between two stars on a free-fall, radial orbit, where shocks can be very important for the dynamics. Here the stars are constantly being held back by a (slowly receding) centrifugal barrier, and the merging, although dynamical, is much more gentle.

After typically 2–3 orbital revolutions the innermost cores of the two stars have merged and the system resembles a single, very elongated ellipsoid. At this point a secondary instability occurs: *mass shedding* sets in rather abruptly. Material is ejected through the outer Lagrange points of the effective potential and spirals out rapidly. In the final stage, the spiral arms widen and merge together. The relative radial velocities of neighboring arms as they merge are supersonic, leading to some shock-heating and dissipation. As a result, a hot, nearly axisymmetric rotating halo forms around the central dense core. The halo contains about 20% of the total mass and the rotation profile is close to a pseudo-barotrope [67], with the angular velocity decreasing as a power-law $\Omega \propto \varpi^{-\nu}$ where $\nu \lesssim 2$ and ϖ is the distance to the rotation axis. The core is rotating uniformly near breakup speed and contains about 80% of the mass still in a cold, degenerate state. If the initial NS had masses close to $1.4M_{\odot}$, then most recent stiff EOS would predict that the final merged configuration is still stable and will not immediately collapse to a black hole, although it might ultimately collapse to a black hole as it continues to lose angular momentum. The emission of gravitational radiation during dynamical coalescence can be calculated perturbatively using the quadrupole approximation (RS). Both the frequency and amplitude of the emission peak somewhere during the final dynamical coalescence, typically just before the onset of mass shedding. Immediately after the peak, the amplitude drops abruptly as the system evolves towards a more axially symmetric state.

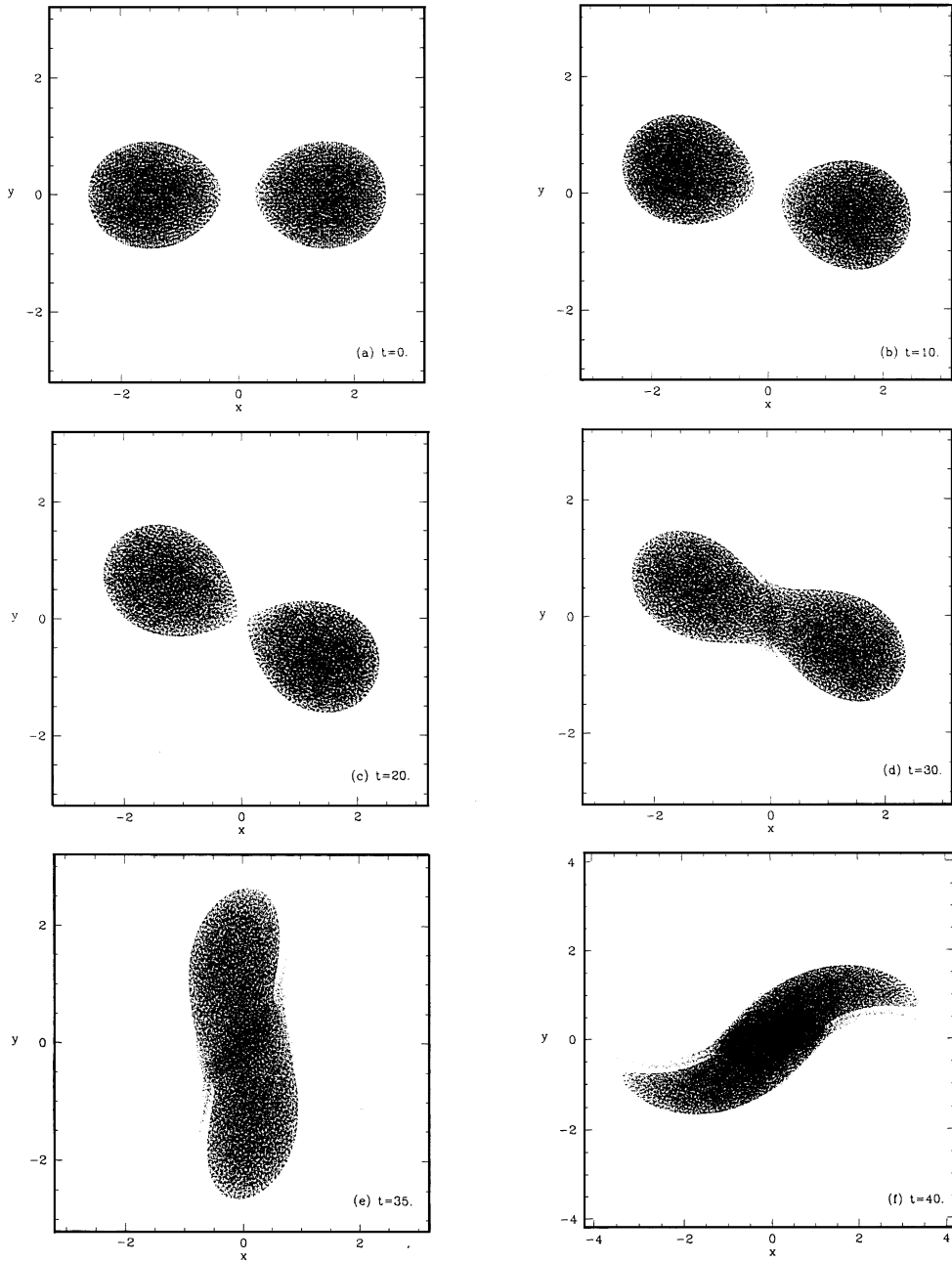


Fig. 2. Evolution of an unstable binary containing two identical neutron stars. The stars are modeled as polytropes with $\gamma=3$, corresponding to a stiff nuclear equation of state. Projections of all SPH particles onto the orbital plane of the binary are shown at different times (the orbital motion is in the counterclockwise direction). Units are such that $G=M=R=1$, where G is the gravitational constant and R and M are the radius and mass of an unperturbed (spherical) star. The initial orbital period is $P_{\text{orb}} \simeq 24$ in these units. Adapted from Rasio and Shapiro [54].

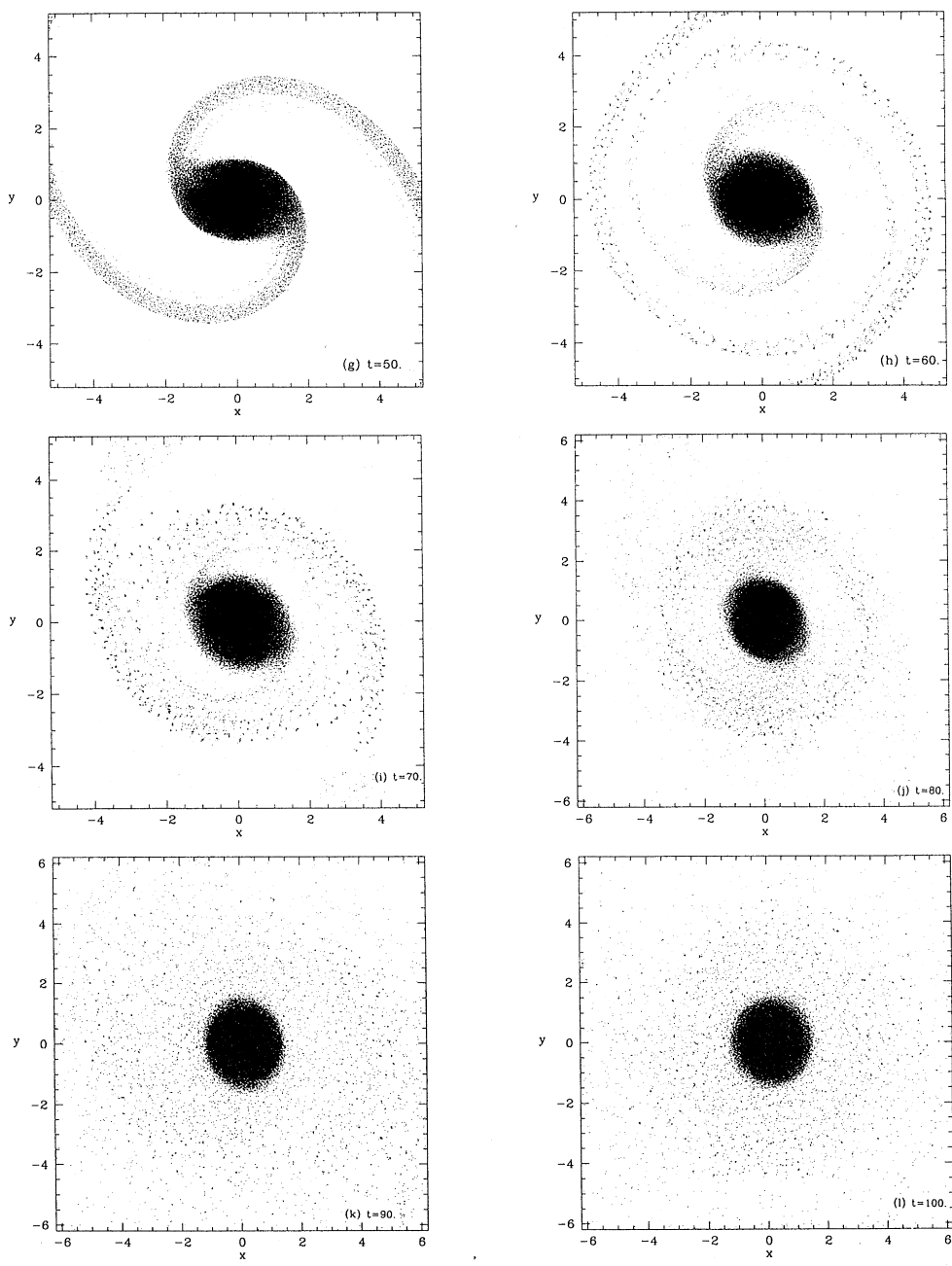


Fig. 2. Continued

References

- [1] M. Abramovici et al., *Science* 256 (1992) 325.
- [2] D. Balsara, *J. Comput. Phys.* 121 (1995) 357.
- [3] M.R. Bate, I.A. Bonnell, *Mon. Not. Roy. Astron. Soc.* 285 (1997) 33.
- [4] W. Benz, J.G. Hills, *Astrophys. J.* 323 (1987) 614.
- [5] W. Benz, J.G. Hills, *Astrophys. J.* 389 (1992) 546.
- [6] C. Bradaschia et al., *Nucl. Instr. and Meth. A* 289 (1990) 518.
- [7] A. Burkert, M.R. Bate, P. Bodenheimer, *Mon. Not. Roy. Astron. Soc.* 289 (1997) 497.
- [8] S. Chandrasekhar, *Astrophys. J.* 202 (1975) 809.
- [9] D.F. Chernoff, L.S. Finn, *Astrophys. J.* 411 (1993) L5.
- [10] H.M.P. Couchman, P.A. Thomas, F.R. Pearce, *Astrophys. J.* 452 (1995) 797.
- [11] C. Cutler et al., *Phys. Rev. Lett.* 70 (1993) 2984.
- [12] K. Danzmann, in: H. Riffert et al. (Eds.), *Relativistic Astrophysics, Proceedings of 162nd W.E. Heraeus Seminar*, Vieweg Verlag, Wiesbaden, p. 48.
- [13] R. Dave, J. Dubinski, L. Hernquist, *New A* 2 (1997) 277.
- [14] M.B. Davies, W. Benz, T. Piran, F.K. Thielemann, *Astrophys. J.* 431 (1994) 742.
- [15] D. Eichler, M. Livio, T. Piran, D.N. Schramm, *Nature* 340 (1989) 126.
- [16] A.E. Evrard, *Mon. Not. Roy. Astron. Soc.* 235 (1988) 911.
- [17] É.E. Flanagan, S.A. Hughes, *Phys. Rev. D* 57 (1998) 4566.
- [18] D. Garcia-Senz, E. Bravo, N. Serichol, *Astrophys. J. Suppl.* 115 (1998) 119.
- [19] R.A. Gingold, J.J. Monaghan, *Astrophys. J.* 181 (1977) 375.
- [20] R.A. Gingold, J.J. Monaghan, *J. Comput. Phys.* 46 (1982) 429.
- [21] H. Goldstein, *Classical Mechanics*, Addison-Wesley, Reading, MA, 1980.
- [22] M. Herant, W. Benz, *Astrophys. J.* 387 (1992) 294.
- [23] L. Hernquist, *Astrophys. J.* 404 (1993) 717.
- [24] L. Hernquist, N. Katz, *Astrophys. J. Suppl.* 70 (1989) 419.
- [25] N. Katz, *Astrophys. J.* 391 (1992) 502.
- [26] N. Katz, D.H. Weinberg, L. Hernquist, *Astrophys. J. Suppl.* 105 (1996) 19.
- [27] R. Klessen, *Mon. Not. Roy. Astron. Soc.* 292 (1997) 11.
- [28] P. Laguna, W.A. Miller, W.H. Zurek, M.B. Davies, *Astrophys. J.* 410 (1993) L83.
- [29] D. Lai, F.A. Rasio, S.L. Shapiro, *Astrophys. J. Suppl.* 88 (1993) 205.
- [30] D. Lai, F.A. Rasio, S.L. Shapiro, *Astrophys. J.* 437 (1994) 742.
- [31] M. Livio, in: R.A. Saffer (Ed.), *ASP Conference Series vol. 53, Blue Stragglers*, San Francisco, ASP, 1993, p. 3.
- [32] J.C. Lombardi Jr., F.A. Rasio, S.L. Shapiro, *Astrophys. J.* 445 (1995) L117.
- [33] J.C. Lombardi Jr., F.A. Rasio, S.L. Shapiro, *Astrophys. J.* 468 (1996) 797.
- [34] J.C. Lombardi Jr., F.A. Rasio, S.L. Shapiro, *Phys. Rev. D* 56 (1997) 3416.
- [35] J.C. Lombardi Jr., F.A. Rasio, A. Sills, S.L. Shapiro, *J. Comput. Phys.*, (1999) in press.
- [36] L.B. Lucy, *Astron. J.* 82 (1977) 1013.
- [37] D. Marković, *Phys. Rev. D* 48 (1993) 4738.
- [38] J.J. Monaghan, *Comput. Phys. Rep.* 3 (1985) 71.
- [39] J.J. Monaghan, *J. Comput. Phys.* 82 (1989) 1.
- [40] J.J. Monaghan, *Annu. Rev. Astron. Astrophys.* 30 (1992) 543.
- [41] J.J. Monaghan, J.C. Lattanzio, *Astron. Astrophys.* 149 (1985) 135.
- [42] T. Naitoh, S. Ono, *Phys. Lett.* 57A (1976) 448.
- [43] R. Narayan, B. Paczyński, T. Piran, *Astrophys. J.* 395 (1992) L83.
- [44] J.F. Navarro, M. Steinmetz, *Astrophys. J.* 478 (1997) 13.
- [45] A.F. Nelson, W. Benz, F.C. Adams, D. Arnett, *Astrophys. J.* 502 (1998) 342.
- [46] R.P. Nelson, J.C.B. Papaloizou, *Mon. Not. Roy. Astron. Soc.* 270 (1994) 1.
- [47] K.C.B. New, J.E. Tohline, *Astrophys. J.* 490 (1997) 311.
- [49] F.A. Rasio, Ph.D. Thesis, Cornell University, 1991.
- [51] F.A. Rasio, in: R. Buccheri et al. (Eds.), *The Many Faces of Neutron Stars*, Dordrecht, Kluwer, 1998, p. 475.

- [52] F.A. Rasio, M. Livio, *Astrophys. J.* 471 (1996) 366.
- [53] F.A. Rasio, S.L. Shapiro, *Astrophys. J.* 401 (1992) 226.
- [54] F.A. Rasio, S.L. Shapiro, *Astrophys. J.* 432 (1994) 242.
- [55] F.A. Rasio, S.L. Shapiro, *Astrophys. J.* 438 (1995) 887.
- [56] M. Ruffert, H.-T. Janka, K. Takahashi, G. Schäfer, *Astron. Astrophys.* 319 (1997) 122.
- [57] B.F. Schutz, *Nature* 323 (1986) 310.
- [58] A. Serna, J.-M. Alimi, J.-P. Chièze, *Astrophys. J.* 461 (1996) 884.
- [59] P.R. Shapiro, H. Martel, J.V. Villumsen, J.M. Owen, *Astrophys. J. Suppl.* 103 (1996) 269.
- [60] S.L. Shapiro, S.A. Teukolsky, *Black Holes, White Dwarfs, and Neutron Stars*, Wiley, New York, 1983.
- [61] M.M. Shara, G. Shaviv, *Mon. Not. Roy. Astron. Soc.* 183 (1978) 687.
- [62] A. Sills, J.C. Lombardi Jr., *Astrophys. J.* 484 (1997) L51.
- [63] A. Sills, J.C. Lombardi Jr., C.D. Bailyn, P. Demarque, F.A. Rasio, S.L. Shapiro, *Astrophys. J.* 487 (1997) 290.
- [64] M. Steinmetz, *Mon. Not. Roy. Astron. Soc.* 278 (1996) 1005.
- [65] M. Steinmetz, E. Müller, *Astron. Astrophys.* 268 (1993) 391.
- [66] M. Tassoul, *Astrophys. J.* 202 (1975) 803.
- [67] J. Tassoul, *Theory of Rotating Stars*, Princeton Univ. Press, Princeton, 1978.
- [68] J.L. Terman, R.E. Taam, *Astrophys. J.* 458 (1996) 692.
- [69] T. Theuns, H.M.J. Boffin, A. Jorissen, *Mon. Not. Roy. Astron. Soc.* 280 (1996) 1264.
- [70] K.S. Thorne, in: J. van Paradijs et al. (Eds.), *Compact Stars in Binaries*, IAU Symposium 165, Kluwer, Dordrecht, 1996, p. 153.
- [72] X. Zhuge, J.M. Centrella, S.L.W. McMillan, *Phys. Rev. D* 54 (1996) 7261.